Statistical Analysis of CFD Solutions from the 6th AIAA CFD Drag Prediction Workshop

Joseph M. Derlaga* and Joseph H. Morrison†
NASA Langley Research Center, Hampton, Virginia, 23681

A graphical framework is used for statistical analysis of the results from an extensive N-version test of a collection of Reynolds-averaged Navier-Stokes computational fluid dynamics codes. The solutions were obtained by code developers and users from North America, Europe, Asia, and South America using both common and custom grid sequencees as well as multiple turbulence models for the June 2016 6th AIAA CFD Drag Prediction Workshop sponsored by the AIAA Applied Aerodynamics Technical Committee. The aerodynamic configuration for this workshop was the Common Research Model subsonic transport wing-body previously used for both the 4th and 5th Drag Prediction Workshops. This work continues the statistical analysis begun in the earlier workshops and compares the results from the grid convergence study of the most recent workshop with previous workshops.

Nomenclature

AR	= aspect ratio
C_D	= total drag coefficient
$C_{D_{PR}}$	= total pressure drag coefficient
$C_{D_{SF}}$	= total skin friction drag coefficient
C_L	= total lift coefficient
C_m	= total pitching moment coefficient
K	= coverage factor for individual values
n	= number of observations in a sample
$NPTS$	= number of solution points in mesh
Re	= Reynolds number based on reference chord
x_i	= value of an observation
$\bar{x}$	= sample mean of a set of observations
$\tilde{x}$	= sample median
μ	= population mean
$\hat{\mu}$	= estimate of the population mean
σ	= population standard deviation
$\hat{\sigma}$	= estimate of the population standard deviation
C_ν	= coefficient of variation ($\hat{\sigma}/\hat{\mu}$)

I. Introduction

In June 2016, the AIAA Applied Aerodynamics Technical Committee (APATC) sponsored the 6th Computational Fluid Dynamics (CFD) Drag Prediction Workshop (DPW-VI) for transonic cruise drag predictions of subsonic transports. The workshop was the most recent follow-on to the first Drag Prediction Workshop (DPW-I) held in June 2001,[1,2] the second Drag Prediction Workshop (DPW-II) held in June 2003,[3,4] the third Drag Prediction Workshop (DPW-III) held in June 2006,[5,6] the fourth Drag Prediction Workshop (DPW-IV) held in June 2009,[7,8] and the fifth Drag Prediction Workshop (DPW-IV) held in June 2012.[9,10]

*Research Scientist, Computational AeroSciences Branch, 15 Langley Blvd. MS 128, AIAA Member
†Chief Engineer for Modeling and Simulation, Research Directorate, 10 West Taylor St. MS 41, AIAA Associate Fellow

The objectives for all the workshops have been (1) to assess the state-of-the-art computational methods as practical aerodynamic tools for aircraft force and moment prediction of industry relevant geometries, (2) to provide an impartial forum for evaluating the effectiveness of existing computer codes and modeling techniques using Reynolds averaged Navier-Stokes solvers, and (3) to identify areas needing additional research and development.

DPW-I solicited CFD predictions of the lift, drag, and pitching moment for the DLR-F4 subsonic transport wing-body (WB) configuration. The DLR-F4 wing-body configuration[11–13] was chosen due to public availability of the geometry and experimental data from three wind tunnels. Test cases consisted of a single point solution at a fixed value of C_L ($C_L = 0.5 \pm 0.0001$), calculation of a drag polar, and an optional calculation of drag rise at constant values of C_L. Grids were made available for participants, but DPW-I did not require a grid convergence study. A total of 38 solutions were submitted for the workshop from 18 authors using 13 different CFD codes. A summary of the results of DPW-I is given in Ref. 1, and a statistical analysis of the results is given in Ref. 2. The code-to-code statistical analysis of the DPW-I results identified two major surprises:[2] (1) roughly 20% of the solutions were statistical outliers compared to the others, and (2) the code-to-code scatter for drag was more than an order of magnitude larger than desired by airframe designers

DPW-II focused on a grid refinement study and the prediction of installed pylon-nacelle drag increments. The DLR-F6[14] wing-body and wing-body-nacelle-pylon (WBNP) configurations were chosen for DPW-II since DLR and ONERA made data publicly available for this configuration. Test cases consisted of a single point solution at a fixed value of C_L ($C_L = 0.5 \pm 0.001$) for both the DLR-F6 WB and WBNP configurations on coarse, medium, and fine grids, and a drag polar. Optional test cases included a comparison of tripped and fully turbulent solutions and calculation of drag rise at fixed values of C_L. A total of 21 solutions were submitted for the workshop from 20 authors using 18 different CFD codes. There were 16 solutions that calculated all three grid levels for both the DLR-F6 WB and WBNP from 15 authors using 15 different CFD codes. A summary of the results is given in Ref. 3, and a statistical analysis of the results is given in Ref. 4. The DLR-F6 configuration had substantial areas of separation at the wing-body juncture and at the wing-pylon juncture. Additionally, there was a region of separation at the trailing edge of the wing. The code-to-code statistical analysis of the DPW-II results identified four major findings:[4,6] (1) roughly 20% of the grid convergence study solutions were statistical outliers, (2) the code-to-code scatter for the wing-body configuration on the medium grid was significantly reduced compared to DPW-I, (3) the code-to-code scatter was still significantly larger than desired by airframe designers, and (4) there was no significant change in code-to-code scatter with increasing grid density.

The panel session discussion at the conclusion of DPW-II identified three suggestions for a third workshop: (1) the large regions of separation were a likely culprit for the lack of grid convergence, therefore, cases should be chosen with minimal separation, (2) simpler cases were required to allow for better grid convergence studies and wider participation, and (3) blind studies were preferable where experimental data were not available *a priori*. It was generally agreed that continuing studies of the DLR-F6 case were warranted. Vassberg et al.[15] designed a side-of-body fairing to produce attached flow in the wing-body juncture. The fairing was designated the FX2B and the configuration was referred to as the DLR-F6-FX2B. An experimental program at DLR and NASA collected data for the DLR-F6 with and without the FX2B fairing.[16] The data were not collected before the workshop and the workshop was run blind. Additionally, two isolated wings, designated DPW-W1 and DPW-W2, were designed[5] to be a simple geometry with DPW-W2 a single point optimization of DPW-W1.

DPW-III focused on grid convergence studies and predicted increments for the DLR-F6 wing-body with and without the FX2B side-of-body fairing. The Reynolds number based on the reference chord was increased to 5 million to minimize the trailing edge separation. The choice of Reynolds number was limited by stress analysis of the wind tunnel model. Additional test cases included a drag polar at fixed Mach number and an optional Reynolds number scaling study. An optional grid convergence study included four grid levels for the DPW-W1 and DPW-W2 isolated wing cases and a drag polar at a fixed Mach number. The isolated wing cases specified the angle-of-attack rather than a fixed C_L. A summary of the DPW-III results is given in Ref. 5, and a statistical analysis is given in Ref. 6. The code-to-code statistical analysis of DPW-III identified four major findings:[6] (1) roughly 20% of the solutions for the grid convergence study of the DLR-F6 wing-body configuration were statistical outliers; none of the solutions for the isolated wings were statistical outliers, (2) the code-to-code scatter for DLR-F6 wing-body fine grid showed no improvement over DPW-II, (3) the code-to-code scatter was still significantly larger than desired by airframe designers, and

(4) the code-to-code scatter showed a reduction with increasing grid resolution when the variation in lift was appropriately accounted for. However, the code-to-code scatter for DPW-III was larger for the coarse and medium grids than for DPW-II.

DPW-IV focused on a grid convergence study and a downwash study including prediction of trimmed drag on the NASA Common Research Model (CRM) wing-body-horizontal tail configuration. Optional cases included a Mach sweep study at fixed C_L and a Reynolds number study. The CRM was a new wing-body-horizontal tail configuration, with and without nacelle-pylons, developed by the NASA Subsonic Fixed Wing (SFW) Aerodynamics Technical Working Group (TWG) in collaboration with the DPW Organizing Committee.[17] The CRM is representative of a contemporary high-performance transonic commercial transport. DPW-IV was a true blind test; the workshop was held in June 2009 and all the data submittals were completed before experimental data were collected. Experimental data were collected in the NASA Langley National Transonic Facility in January-February 2010 and in the NASA Ames 11-by 11-Foot Transonic Wind Tunnel during March-April 2010.[18] A summary of the results from DPW-IV is provided in Ref. 7.

The code-to-code statistical analysis of DPW-IV identified five major findings:[8] (1) roughly 12.5% of the solutions for the grid convergence study were outliers, (2) the code-to-code scatter for the total drag, normalized by the total drag to account for different drag levels between cases was virtually the same for DPW-II, DPW-III, and DPW-IV, (3) the code-to-code variation of the forces and pitching moment, normalized by the appropriate force or pitching moment, was substantially larger on the horizontal tail component than on the wing or fuselage component, (4) the code-to-code variation was still substantially higher than desired by airframe designers, and (5) the drag (total drag, pressure drag, and skin friction drag) showed some reduction in scatter with increasing grid resolution.

DPW-V focused on a grid convergence study using a common set of grids for all CFD codes. A five block multiblock grid around the CRM wing-body was developed with six grid levels ranging from approximately 639 thousand grid points on the coarsest grid to over 138 million points on the finest grid.[9] This multiblock grid was converted to overset, unstructured hexahedral, unstructured prisms, and unstructured hybrid grids using the exact same set of grid points. Optional cases included a wing-body buffet study at fixed Mach and a turbulence model verification study. A summary of results from DPW-V is provided in Ref. 9.

The statistical analysis of DPW-V identified three major findings:[10] (1) the code-to-code scatter of the total drag, pressure drag, and the skin friction drag was substantially lower than earlier workshops and decreased with increasing grid resolution, (2) the code-to-scode scatter in the pitching moment did not show a convergent trend with increasing grid resolution, and (3) roughly 16% of the solutions for the grid convergence study were outliers.

Discussion at the conclusion of DPW-V recommended continuing the workshop series with continuing focus on the CRM. DPW-VI focused on a verification study, predicting the drag increment for the nacelle-pylon, and predicting the static aeroelastic effect for an angle of attack sweep using the aeroelastic deflection measured in the wind tunnel, as Rivers et al.[19] and Hue[20] demonstrated the impact of static aeroelastic deflection for the CRM after DPW-V. The static aeroelastic effect for an angle of attack sweep required substantially more grid generation work as each angle of attack had a different geometry corresponding to the aeroelastic deflection. Optional cases included a grid adaption case and a coupled aerostructural simulation. This paper focuses on a statistical analysis of the grid convergence study for the nacelle-pylon increment.

This paper is organized in the following manner. Section II provides a description of the statistical analysis. Section III outlines the test cases for the workshop. Section IV details the statistical results. Section V provides some summary comments.

II. Statistical Approach

Hemsch[2] introduced the idea of treating different computations of a test case as a collective and using N-version testing in a statistical framework to investigate the submissions. No individual result is considered the right or best result. This framework is useful for identifying differences between submissions. The dispersion of the results is treated as noise in the collective computational process.

A running record of individual outcomes is plotted for each of the measures of interest and derived quantities reported by participants. Participants reported several quantities including angle of attack (α), total drag coefficient (C_D), pressure drag coefficient ($C_{D_{PR}}$), skin friction drag coefficient ($C_{D_{SF}}$), and pitching moment coefficient (C_m). The value of the measure of interest is plotted on the vertical axis and a

unique integer index is used for each data submission on the horizontal index. The order of the solutions on the horizontal axis is irrelevant since this is not a temporal axis.

An estimate of the population mean $\hat{\mu}$ of the plotted data submissions is made and is shown on the graph as the centerline. Upper and lower scatter limits are placed on the graph as follows:

$$\text{Upper Limit} = \hat{\mu} + K\hat{\sigma} \tag{1}$$

$$\text{Lower Limit} = \hat{\mu} - K\hat{\sigma} \tag{2}$$

where $\hat{\sigma}$ is an estimate of the population standard deviation and K is an appropriate coverage factor. Significant results are outcomes that lie outside the process limits defined in Eqs. (1) and (2). These results, referred to as outliers, represent submissions that are different from the results that lie within the scatter limits (and should be investigated to understand the difference).

The population mean $\hat{\mu}$ is estimated using the sample median, which is given (for sorted data) as:

$$\hat{\mu} = \tilde{x}$$

$$\tilde{x} \equiv x_{(n+1)/2} \quad \text{for odd n} \tag{3}$$

$$\tilde{x} \equiv 0.5(x_{n/2} + x_{(n/2)+1}) \quad \text{for even n}$$

The sample median provides a robust estimate when outliers are present. The sample standard deviation

$$\hat{\sigma} = SSD \equiv \sqrt{\frac{1}{n-1}\sum_{i=1}^{n}(x_i - \bar{x})^2} \tag{4}$$

is used to estimate the population standard deviation. The coverage factor is estimated for a uniform distribution as $K = \sqrt{3}$.[21] This value of coverage factor was chosen to look for differences in submissions based on past workshop experience.

For this workshop, a different method of graphically examining the submitted results has been developed. Figure 1(a) shows a combination of a violin plot with a box-and-whisker (with notch)[22] plot overlay. The violin plot represents the sample distribution, indicating the levels of solution clustering and behavior of the tails of the data. The box-and-whisker plot groups data by quartiles and indicates outliers. At the neck of the box plot is the sample median, while the upper and lower limits of the box represent the upper and lower quartiles (medians of the upper and lower 50% of the data). The notch around the median is included to aid in comparisons of the median values between different grid levels; nonoverlapping notches are indicative of a significant difference between the median values. The distance between the upper and lower bounds of the box is referred to as the interquartile range (IQR), and contains 50% of the submitted data. The whiskers represent the maximum and minimum values outside of the IQR; however, if the maximum or minimum values lie outside the value of 1.5xIQR added or subtracted to the upper or lower quartiles, respectively, then the whiskers represent the maximum or minimum values that are considered statistically significant. Values that are outside the 1.5xIQR limit are shown as solid blue circles. In addition, the sample mean is plotted as a solid blue diamond. The horizontal axis shows the grid level and the number of submissions received at that grid level.

Figure 1(b) is a scatter plot of the same data submissions as in Fig. 1(a), and includes the median as a solid line and upper and lower scatter limits, $\hat{\mu} \pm K\hat{\sigma}$, as dotted lines. Note that apparent outliers in Fig. 1(b) are not always treated as outliers in Fig. 1(a). The dotted line in Fig. 1(b) should be interpreted as a relatively broad line, and in order for an outlier to truly be considered an outlier, it must fall significantly outside the range of the scatter limits.

III. DPW-VI Test Cases

Unique to DPW-VI compared to past drag prediction workshops, a code verification study was required of all participants. A subsonic, 2D, NACA 0012 from the Turbulence Modeling Resource was studied as Case 1. More details can be found in Roy.[23]

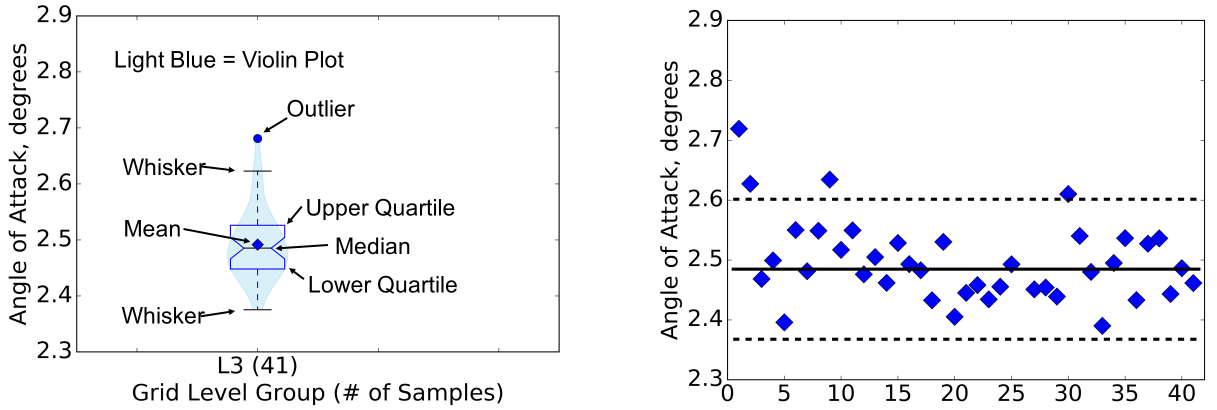

(a) Sample violin/box-and-whisker plot

(b) Sample scatter plot

Figure 1: Comparison of new summary plot with corresponding scatter plot.

Cases 2 through 5 all studied the geometry of the Common Research Model (CRM) as described in Vassberg et al.[17] For these studies, the reference conditions were freestream Mach = 0.85, Re = 5 million, and temperature = 100 $^\circ F$, in free air, i.e., no wind tunnel walls or model mounting systems were included. Boundary layers were modeled as fully turbulent.

Structured overset and unstructured grids were made available by the organizing committee; custom grid systems were welcome. The unstructured grid system was designed for cell vertex schemes and therefore, resulted in a much higher number of degrees of freedom when used by cell-centered codes. Six grid levels were provided (L1 through L6), starting at approximately 20 million nodes for the wing-body (WB) geometry (approximately 25-30 million for the wing-body-nacelle-pylong (WBNP) geometry) and increasing by approximately 1.5x in total vertex count for each subsequent grid level. The coarsest grid level was designed to ensure a viscous wall spacing (y^+) of approximately 1.

A grid convergence study on the middle four grid levels (L2 through L5) was performed for Case 2A and Case 2B. An α-seek was performed in order to match a desired loading condition of $C_L = 0.5 \pm 0.0001$, using a geometry modified for aeroelastic deflection at $\alpha = 2.75^\circ$. Case 2A consisted of a WB geometry, while Case 2B added an engine nacelle and pylon (WBNP) to the geometry of Case 2A in order to understand the predicitive capabilities of the various CFD tools in calculating drag increments between configurations.

Case 3 performed an α sweep study of a model that had undergone static aeroelastic deflections at various angles of attack. In examining previous workshop results, the incorrect definition of wing twist from the as built model and lack of aeroelastic deflections in the workshop grids was found to seriously hamper comparisons with experimental data.[19,20]

Cases 4 and 5 were optional, involving a grid adaptation study of the Case 2A configuration, and a coupled aerostructural simulation of the Case 2A geometry, respectively.

The main focus of this paper is on the results for Case 2A and 2B. Before a detailed analysis was made, an initial study of the submissions identified several outliers. As an example, the total drag coefficient for Case 2B for all submissions on the L3 grid level are shown in Fig. 2(a).

Submissions 43, 44, and 45 were found to have not performed the α-seek in order to match the $C_L = 0.5$ condition and were therefore removed from the statistical analysis. This left one outlier, as shown in Fig. 2(b). Submission 42 utilized a Spalart-Allmaras (SA) turbulence model, which has been shown in past workshops to suffer from side of body separation, and which was not fully converged on all submitted grid levels. As a result, it has been removed from the statistical analysis as it greatly skews the statistical results. Upon removal of submission 42, the confidence bands have been greatly reduced for all quantities of interest, as shown in Fig. 2(c). All remaining outliers are discussed in detail below.

IV. Results

The data were submitted to the DPW committee before the workshop. After the workshop, authors were given time to evaluate and resubmit their solutions. Several authors took advantage of this time and

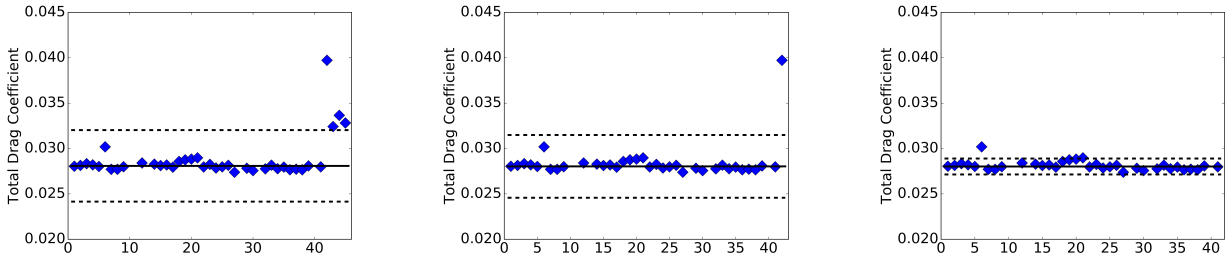

(a) All submissions (b) Submissions with α-seek (c) Last outlier removed

Figure 2: Characteristic outlier removal based on C_D for Case 2B, L3 grid level.

submitted corrections to their solutions or provided additional data that they did not have time to complete before the workshop. Within the following sections, summary violin/box-and-whisker plots will be shown. These summary plots will be shown side-by-side for Cases 2A and 2B in order to quickly see the trends in the changes of the quantities of interest between the two problems. Scatter plots (including scatter limits) of a quantity of interest vs. submission number, such as those shown in Fig. 1(b) above, are included in the appendix. Outliers identified in the box-and-whisker plots will be refered to by their integer submission number from the scatter plots.

IV.A. General Summary for Cases 2A and 2B

The IQR for all of the drag coefficients, shown in Fig. 3 through Fig. 5, is universally on the order of four to five drag counts (1 count = 0.0001 C_D), with the scatter limits reducing by approximately one to two counts per grid level, indicating that while approximately 50% of the submissions were tightly clustered about the median, most of the improvement in reducing the scatter bounds comes from convergence of outliers toward the median. This is not to say that the value of the median doesn't change with grid refinement; just that close to 50% of the data closely tracks the median with grid refinement. Angle of attack, Fig. 6, and pitching moment, Fig. 7, show a similarly constant IQR with grid refinement.

On the finer grid levels, where there are fewer submissions, the IQR typically reduces for the three drag coefficients, but not for the other two quantities. In addition, there were typically 10% to 20% fewer submissions for Case 2B than Case 2A.

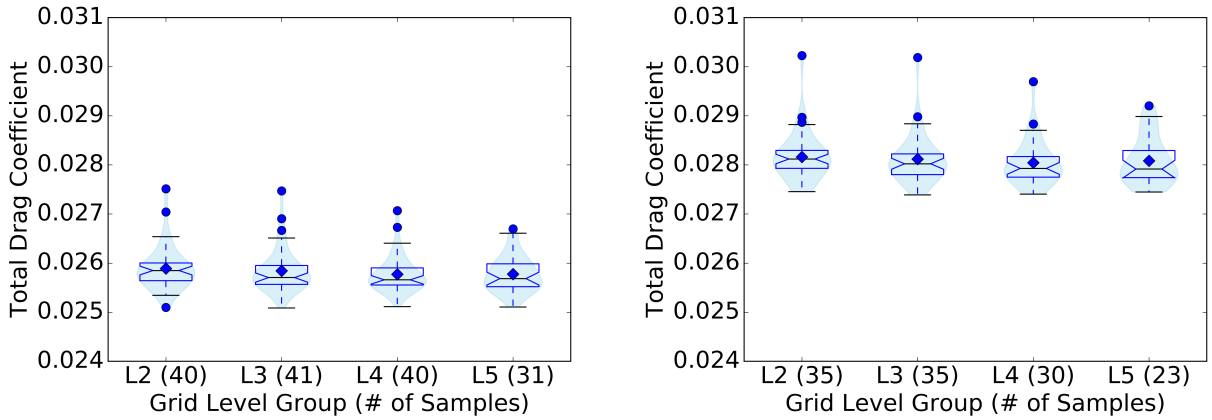

(a) Case 2A (b) Case 2B

Figure 3: Summary of C_D.

Summaries of the medians and standard deviations for Cases 2A and 2B can be found in Table 1 through Table 4. The presence of the nacelle and pylon increase the standard deviation in the drag by less than a count. Compared to the standard deviations computed for DPW-V,[10] the results from DPW-VI show higher deviation for almost all quantities, but this can be attributed to the fact that a common grid

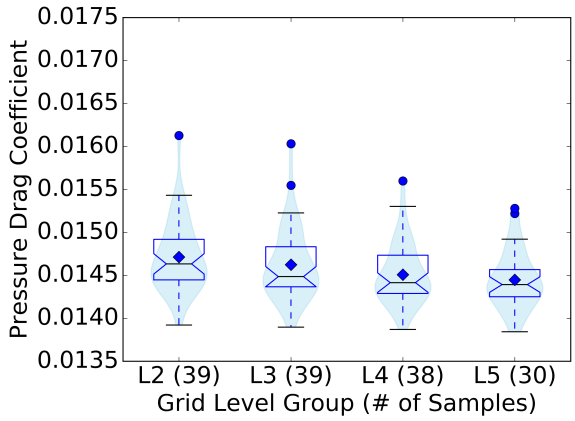

(a) Case 2A

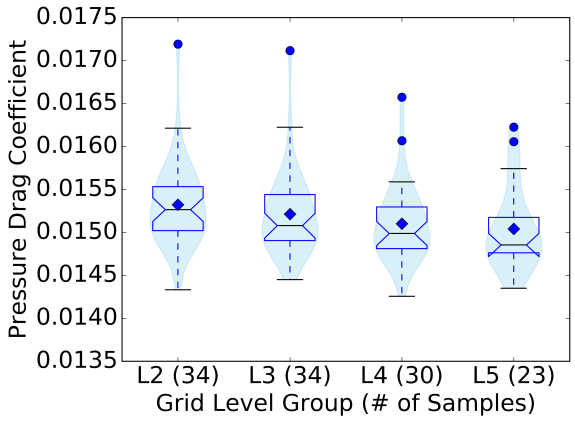

(b) Case 2B

Figure 4: Summary of $C_{D_{PR}}$.

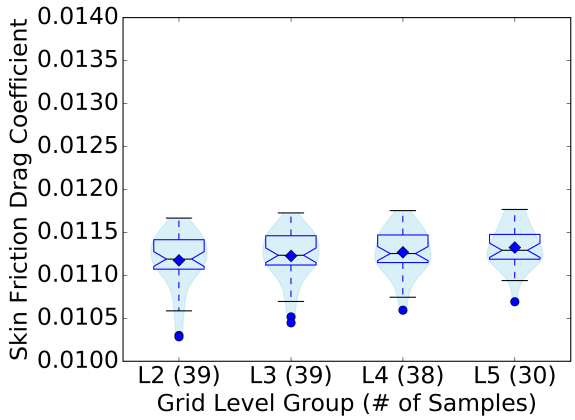

(a) Case 2A

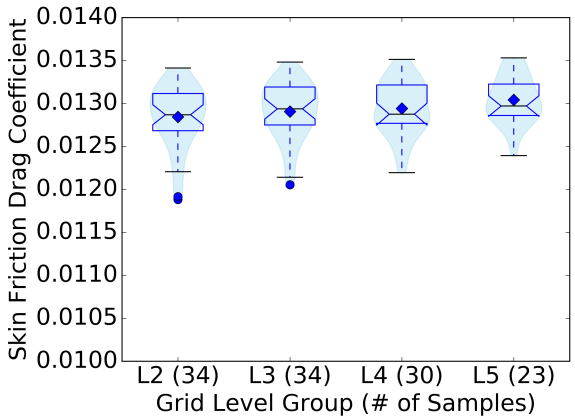

(b) Case 2B

Figure 5: Summary of $C_{D_{SF}}$.

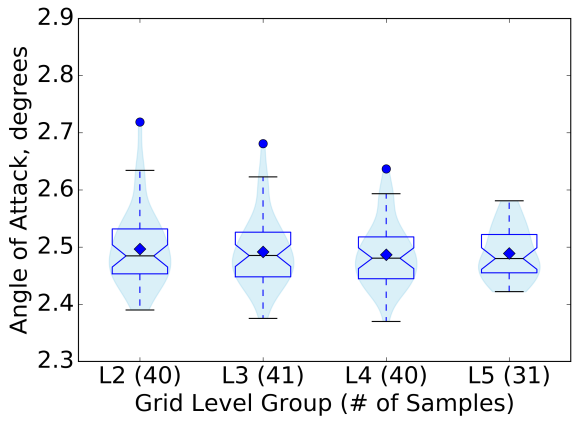

(a) Case 2A

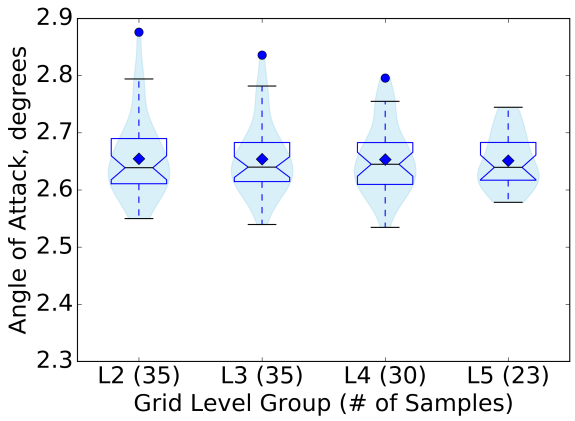

(b) Case 2B

Figure 6: Summary of α.

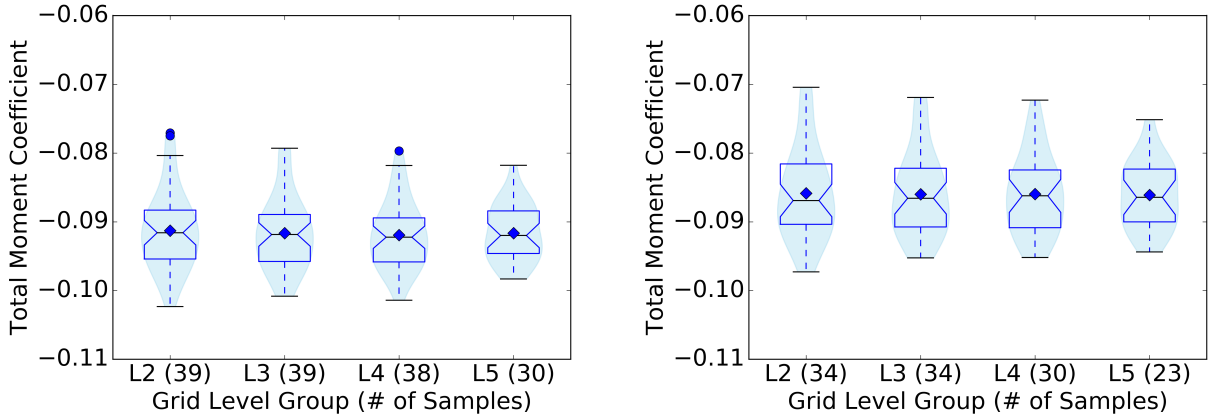

(a) Case 2A

(b) Case 2B

Figure 7: Summary of C_m.

sequence was used by the majority of DPW-V submissions. Overall, the medians of the various drag coefficients change very little with grid refinement, with only the skin friction drag for Case 2B showing a change of more the 2 counts, which is well within the standard deviation for that quantity.

Table 1: Comparison of Case 2A medians.

	Coarse (L2)	Medium (L3)	Fine (L4)	Extra Fine (L5)
α, degrees	2.485	2.485	2.481	2.480
C_D, counts	258	257	257	257
$C_{D_{PR}}$, counts	146	145	144	144
$C_{D_{SF}}$, counts	112	112	113	113
C_m	-0.0916	-0.0919	-0.0922	-0.0920

Table 2: Comparison of Case 2A standard deviations.

	Coarse (L2)	Medium (L3)	Fine (L4)	Extra Fine (L5)
α, degrees	0.067	0.062	0.056	0.046
C_D, counts	4.5	4.4	3.7	3.7
$C_{D_{PR}}$, counts	4.1	4.2	3.5	3.4
$C_{D_{SF}}$, counts	3.3	2.9	2.6	2.5
C_m	0.0058	0.0055	0.0049	0.0041

Table 3: Comparison of Case 2B medians.

	Coarse (L2)	Medium (L3)	Fine (L4)	Extra Fine (L5)
α, degrees	2.639	2.640	2.645	2.640
C_D, counts	281	280	279	279
$C_{D_{PR}}$, counts	153	151	150	149
$C_{D_{SF}}$, counts	129	129	129	130
C_m	-0.0869	-0.0866	-0.0862	-0.0864

Table 4: Comparison of Case 2B standard deviations.

	Coarse (L2)	Medium (L3)	Fine (L4)	Extra Fine (L5)
α, degrees	0.071	0.064	0.061	0.049
C_D, counts	5.1	5.0	4.7	4.9
$C_{D_{PR}}$, counts	5.0	4.9	4.5	4.8
$C_{D_{SF}}$, counts	3.7	3.3	3.1	2.8
C_m	0.0068	0.0062	0.0058	0.0049

IV.B. Summary of Outliers for Cases 2A and 2B

Beginning with angle of attack, one statistically significant outlier is identified on grid levels L2 through L4 for both Cases 2A and 2B (submission 1 as seen in the Appendix). Total pitching moment indicates no outliers for Case 2B due to a larger IQR, but two on the L2 grid level (submissions 1 and 9) and one on the L4 grid level (submission 8) for Case 2A. In general, submissions that had found a higher angle of attack in order to match C_L also had higher pitching moments. For total drag coefficient, submission 6 was the highest outlier for all cases, while submission 11 was second highest for Case 2A on the L2-L4 levels, with submission 21 third highest for Case 2A on the L3 level. For Case 2B, submission 21 was the second highest outlier on the L2-L4 levels, while submission 19 was the third highest outlier on the L2 grid level. As with C_D, the pressure drag had outliers from submissions 6 and 21 for both cases; submission 6 was the highest outlier for grid levels L2-L4, while submission 21 became the highest for the L5 level. For skin friction drag, submission 27 has the lowest skin friction across all grid levels for both cases (although it is not statistically significant for the L4 and L5 grid levels for Case 2B) followed by submission 8 on the L2 and L3 levels of Case 2A and the L2 level for Case 2B.

Submission 1: While generally showing the highest angle of attack, this submission typically also had a lower magnitude of the pitching moment, close to that of submission 8. Also, while the skin friction value was typically lower than the median, the predicted pressure drag was higher, resulting in total drag coefficients that closely tracked the median. This submission was unique in that it used the k-kL-MEAH2015 turbulence model and used the workshop provided grid system. Submissions 1 and 2 were contributed by the same group, differing only in the use of a reconstruction limiter for the finite volume scheme for submission 2, whereas submission 1 had no such limiter. Submission 2 fell within the scatter limits, but tended to have higher values of angle of attack and lower magnitudes of pitching moment. The difference in turbulence model could well account for the differences between all other submissions.

Submission 6: This submission was typically highest in both total drag and pressure drag, but was within the scatter bounds for all other quantities. An SST-$k\omega$ (Shear Stress Transport) turbulence model was used on custom grids which were much finer, often by a factor of 3x, than the requirements given in the gridding guidelines for the workshop. The solver uses a cell-centered, pressure based approach, which is unique from all other submissions, and may account for the statistical differences.

Submissions 8 and 9: These submissions were from the same group; submission 8 was unique in that it was the sole submission that used an EARSM (Explicit Algrebraic Reynolds Stress Model) and submission 9 used a standard SA model, both on workshop provided grids. Both submissions typically had higher angles of attack and lower pitching moment magnitudes, even if not statistically significant using the IQR criteria. The EARSM also tended toward having a lower skin friction coefficient. It should be noted that all boundary conditions (including walls) for these submissions are weakly enforced and could therefore account for the differences compared to other solutions.

Submission 19: While considered a statistically significant outlier for the total drag for Case 2B on the L2 grid level, submission 19 is generally within the bounds of the scatter limits, but does tend to have a higher value of pressure drag with grid refinement. This submission used an SST turbulence model on Boeing provided unstructured grids.

Submission 21: This submission also used the Boeing provided unstructured grids, but was contributed by another group than that of submission 19. An SA-noft2-QCR2000 turbulence model was used for this submission, but the same group used the same turbulence model and their own grid for submission 25 and fell well within the scatter limits. In addition, this group also contributed submission 20, which used an

SA-noft2 model, and also fell within the scatter limits. This may imply that the Boeing provided grid may be unsuitable for this solver when using the SA-noft2-QCR2000 model.

Submission 27: A cell-centered flow solver using an SA turbulence model on custom grids that followed the gridding guidelines was used for this submission. This has resulted in this submission having the lowest values of skin friction and total drag for both cases at all grid levels. There were no signs of premature side-of-body separation and all cases appeared to be well converged. There was no identified reason why this submission resulted in low values of skin friction and total drag despite having reasonable pressure drag.

IV.C. Delta of Quantities Between Cases 2A and 2B

This workshop provided the ability to study the drag buildup (Δs) between the CRM WB and CRM WBNP configurations; violin/box-and-whisker summary plots for the three drag coefficient quantities are provided in Fig. 8(a) through Fig. 8(c), where the results of Case 2A are subtracted from the results of Case 2B. While the spread between the whiskers for the drag coefficients for Cases 2A and 2B were on the order of 10 to 15 counts, the spread between the whiskers for the Δs are on the order of 5 counts or less. The IQR is also approximately reduced by a factor of three for each of the drag coefficient quantities as well. While no outliers exist for $C_{D_{SF}}$, the submissions appear to follow a bimodal distribution, and the overall range between all the submissions is generally on the order of 2 counts.

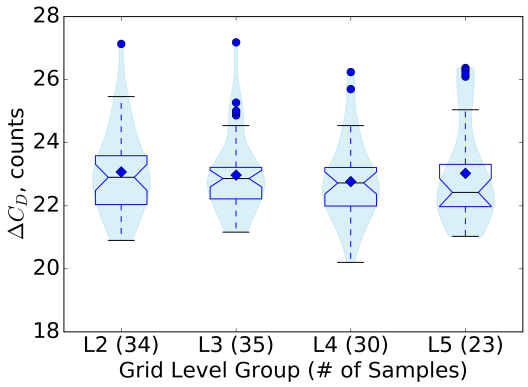

(a) Δ C_D

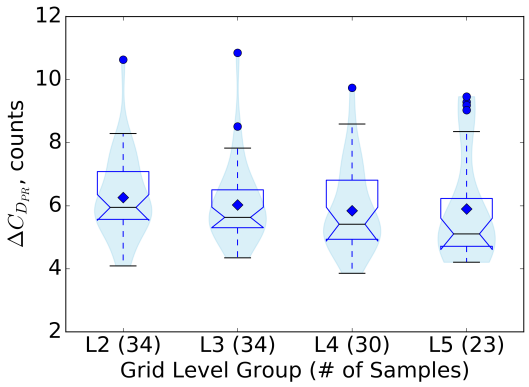

(b) Δ $C_{D_{PR}}$

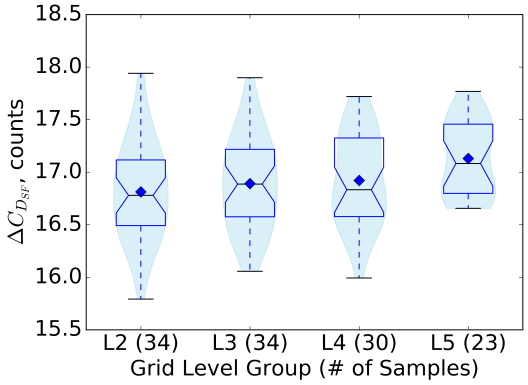

(c) Δ $C_{D_{SF}}$, note different range than (a) and (b)

Figure 8: Summary of Δ's of drag coefficients.

Outliers in $C_{D_{PR}}$ typically result in higher values of total drag. Submission 6 is the highest outlier for total drag and pressure drag on all grid levels except on grid level L5, at which point submission 18, 19, 20, and 21 all become higher. Submissions 6 and 21 (and by extension 20) were discussed above. Submssion 19 was also discussed above, and was contributed by the same group as submission 18. Even though submission 18 was the median value of $C_{D_{PR}}$ for Case 2A, it appears that the pressure drag computed for Case 2B was just high enough to become significant. On the L3 grid level, submission 33 also appears as an outlier

for total drag and pressure drag. Submission 33 utilized a custom-hybrid grid system for a node-based finite-volume solver with an SST turbulence model; other submissions from the same group with the same turbulence model were not statistically outliers. As with submission 18, the median value for pressure drag on Case 2A was well matched and the computed value on Case 2B was slightly higher.

Also appearing as outliers on the L3 grid level for total drag are submissions 3 and 26. Submission 3 matched the median value of total drag for Case 2A, but was higher than the median on Case 2B. Unfortunately, submission 26 did not include a drag breakdown in order to determine the contributions from pressure and skin friction drag. Solution 18 is also a total drag outlier on the L4 grid level for the same reasons as noted above for the L5 grid level.

As with Cases 2A and 2B, summaries of the medians and standard deviations are given in Table 5 and Table 6. While skin friction drag accounts for almost 75% of the ΔC_D, it is subject to far less deviation than the pressure drag, which in turns drives the deviation in the total drag. While ΔC_D and $\Delta C_{D_{PR}}$ show a slight decrease with grid refinement, $\Delta\alpha$, ΔC_m, and $\Delta C_{D_{SF}}$ do not. As shown with the violin/box-and-whisker plots above, the Δs of quantities between configurations are somewhat constant with respect to grid level, even if the predicted magnitudes of those quantities are not.

Table 5: Comparison of medians of differences.

	Coarse (L2)	Medium (L3)	Fine (L4)	Extra Fine (L5)
$\Delta\alpha$, degrees	0.161	0.164	0.162	0.161
ΔC_D, counts	22.9	22.9	22.7	22.4
$\Delta C_{D_{PR}}$, counts	5.9	5.6	5.4	5.1
$\Delta C_{D_{SF}}$, counts	16.8	16.9	16.8	17.1
ΔC_m	0.0056	0.0058	0.0057	0.0056

Table 6: Comparison of standard deviations of differences.

	Coarse (L2)	Medium (L3)	Fine (L4)	Extra Fine (L5)
$\Delta\alpha$, degrees	0.007	0.007	0.005	0.005
ΔC_D, counts	1.39	1.29	1.31	1.71
$\Delta C_{D_{PR}}$, counts	1.32	1.29	1.36	1.79
$\Delta C_{D_{SF}}$, counts	0.47	0.45	0.44	0.35
ΔC_m	0.0009	0.0007	0.0007	0.0007

IV.D. Comparison of DPW-VI results with DPW-II through DPW-V

DPW-II through DPW-V each included a grid convergence study. Gridding guidelines were posted before each workshop and included recommended sizes for each of the grids in the grid convergence studies to provide a guide to the participants. For DPW-V and DPW-VI, grids were provided by the committee Grid sizes tripled over the course of these three workshops. However, the question remains whether increasing grid sizes have improved the results.

The coefficient of variation,[24] $C_\nu = \sigma/\mu$, provides a measure to compare the variation of populations with different means. The results of DPW-VI are compared to the results of DPW-II,[4] DPW-III,[6] DPW-IV,[8] and DPW-V[10] for the cases that were run at constant lift. Morrison and Hemsch[6] showed that the variation in lift affected the comparisons of drag quantities and pitching moment and showed that quantities that corrected to a constant lift condition, e.g., L/D and idealized profile drag, were required to compare results at different values of lift.

The coefficient of variation for the pitching moment coefficient would be negative since the mean is negative and the estimate of the standard deviation is positive. Therefore, $|C_\nu|$ is plotted for the pitching moment coefficient to make comparisons easier.

The coefficients of variation for the total drag, pressure drag, skin friction drag, and pitching moment coefficients are shown in Figs. 9-12 for DPW-VI and earlier workshops. This variation includes different

turbulence models, different codes and numerics, different participants, different forms of the Common Grid Sequence grids, and even a few custom grids. Table 7 reports the number of submission for grid levels L1 through L6 for both Cases 2A and 2B of DPW-VI.

Table 7: Total submission counts for Case 2A and Case 2B.

	Case 2A	Case 2B
L1	41	34
L2	40	35
L3	41	35
L4	40	30
L5	31	23
L6	22	13

Compared to DPW-V, the variation in the DPW-VI results are universally higher for similar grid complexity. The variation for Case 2A is lower than the variation for Case 2B, but the L6 grid level for Case 2B had a median value of the grid size that was lower than the L5 grid level, and also lower than the L6 grid size for Case 2A. One possible reason for this is that those who could afford to run a sixth grid level also had to use coarser resolutions at the lower grid levels, as compared to those using the workshop suggested guidelines for number of grid points. Despite this, the total variation in all the drag coefficients is actually lower for Case 2B on the L6 grid level compared to the L5 grid level, whereas the opposite is true for the drag coefficients for Case 2A. In general, the total variation for Case 2A shows increased variation at the L6 grid level, and this is most likely due to the decreased number of submissions. The pitching moment variations are also higher than the DPW-III results, but converge at a much faster rate vs. number of grid points.

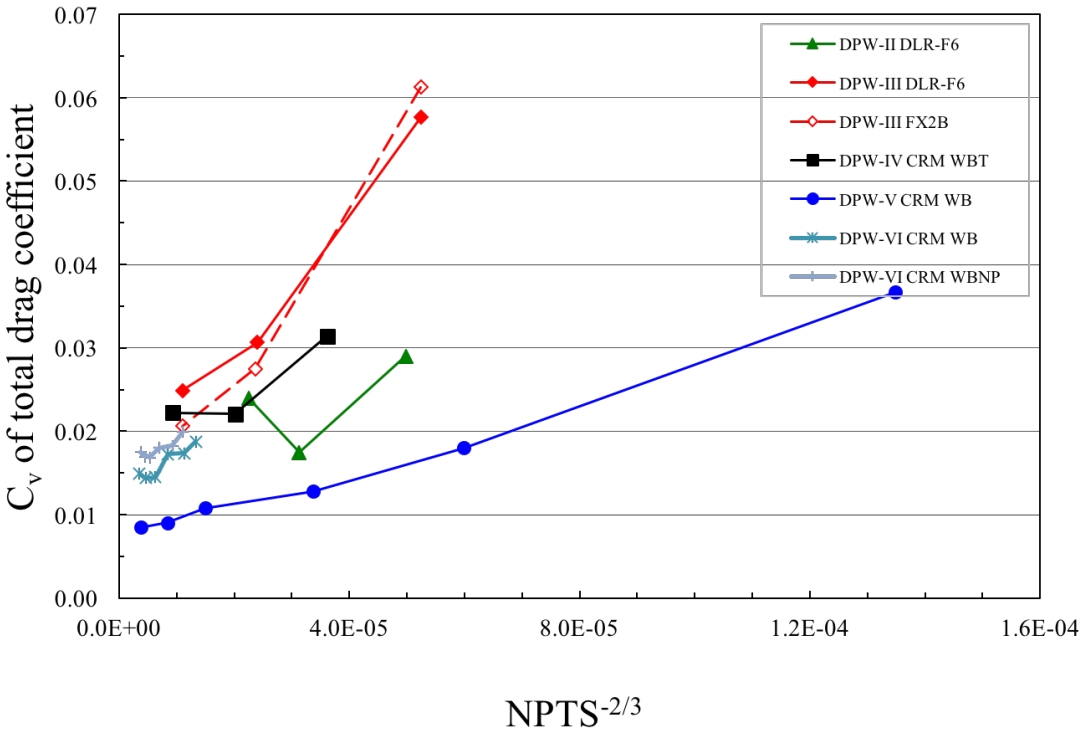

Figure 9: Coefficient of variation of the total drag coefficient.

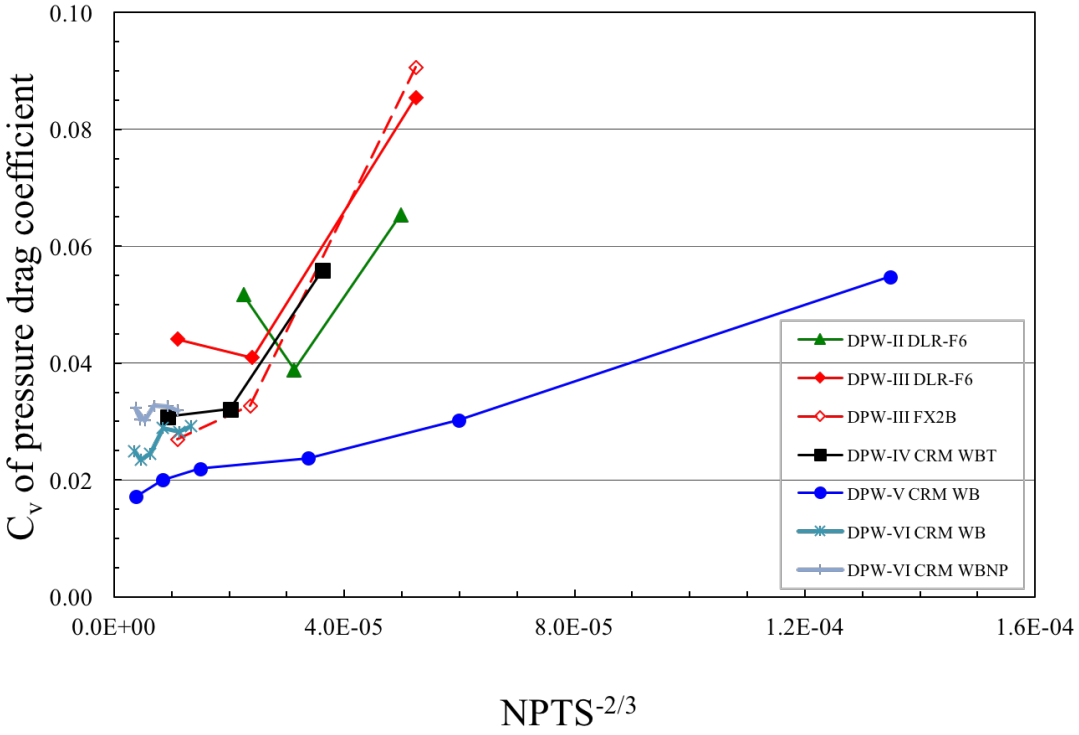

Figure 10: Coefficient of variation of the pressure drag coefficient.

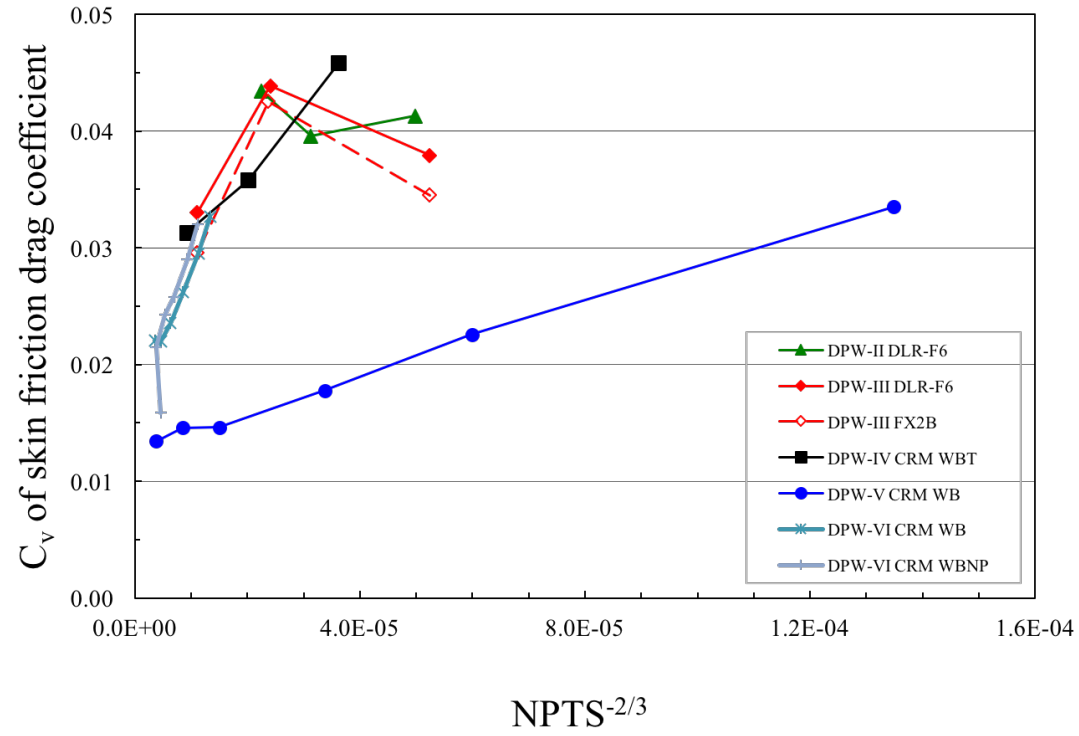

Figure 11: Coefficient of variation of the skin friction drag coefficient.

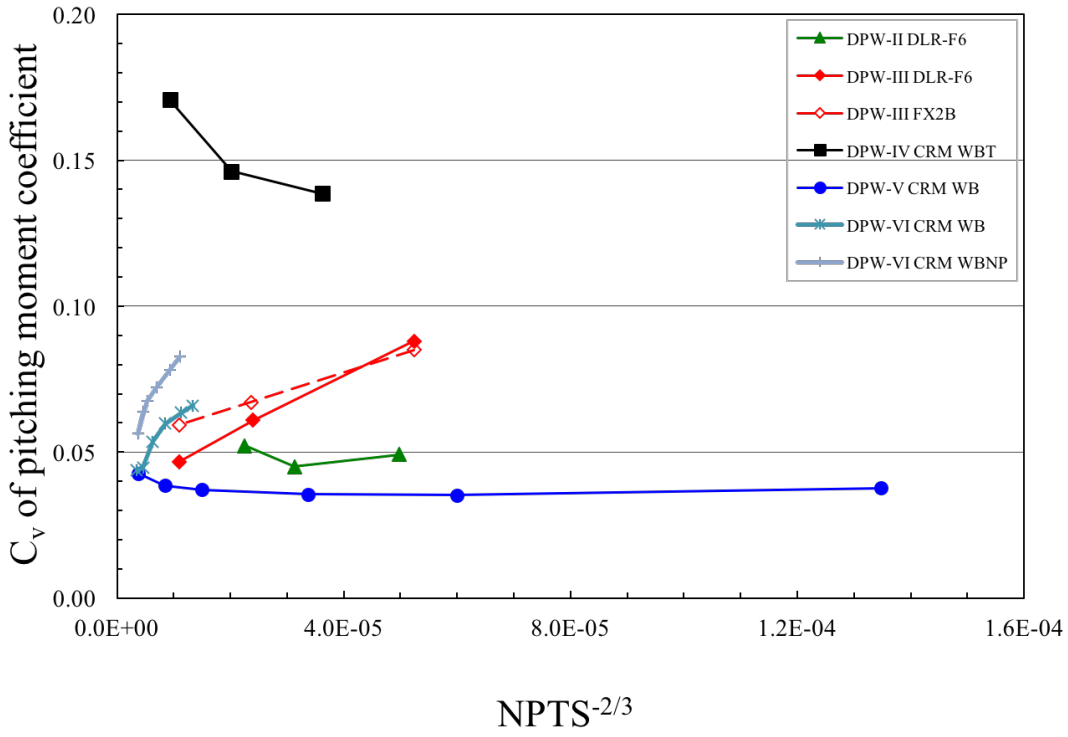

Figure 12: Coefficient of variation of the magnitude of the pitching moment coefficient.

V. Conclusions

A statistical analysis, including a new presentation of the submission statistics and outliers, was applied to the results of the 6th AIAA CFD Drag Prediction Workshop. The code-to-code scatter of the total drag coefficient, pressure drag coefficient, and skin friction drag coefficient were substantially higher than for DPW-V, but in line with the scatter from DPW-II through DPW-IV. The lower level of scatter in DPW-V was from the use of the Common Grid Sequence; DPW-VI did not use a common grid and reverted to scatter levels similar to other workshops that also did not use a common grid. However, the drag coefficients did not exhibit a smooth convergence trend and additional analysis of the individual submissions and grids will be required to identify the cause of this behavior. The statistical analysis of the grid convergence study showed approximately 18% of the submissions were outliers, which is consistent with earlier workshops. In addition, the delta between the wing-body and the wing-body-nacelle-pylon configuration had lower levels of scatter than the absolute values. The drag coefficient scatter for the delta between configurations was on the order of a few counts of drag.

Appendix

This page has been left intentionally blank. The figures on the following several pages are all formatted in the same manner, between grid level and case, to allow for visual differencing of solutions.

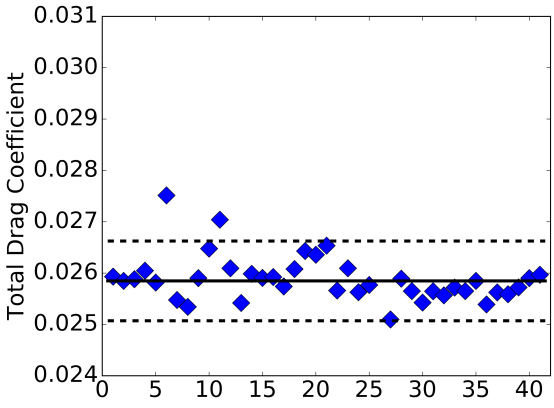

(a) Total drag coefficient

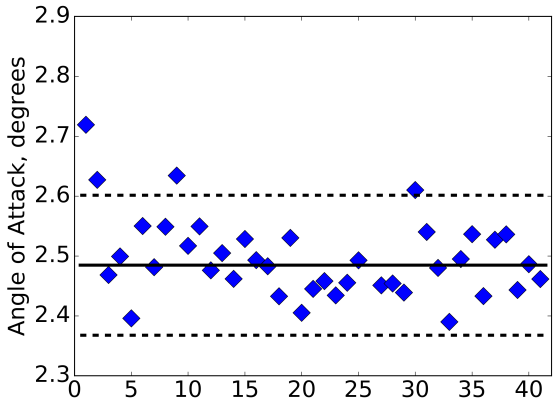

(b) Angle of attack

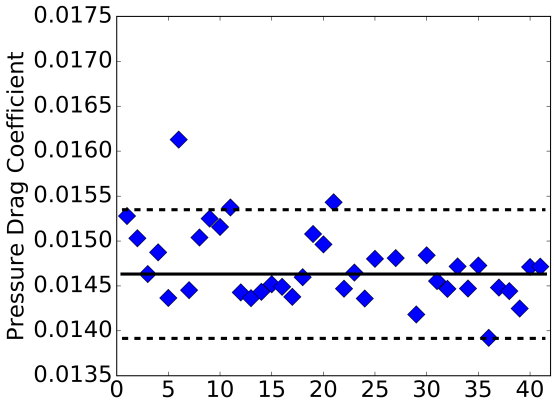

(c) Pressure drag coefficient

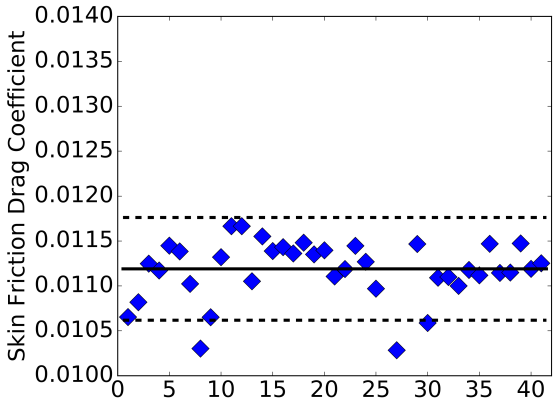

(d) Skin friction drag coefficient

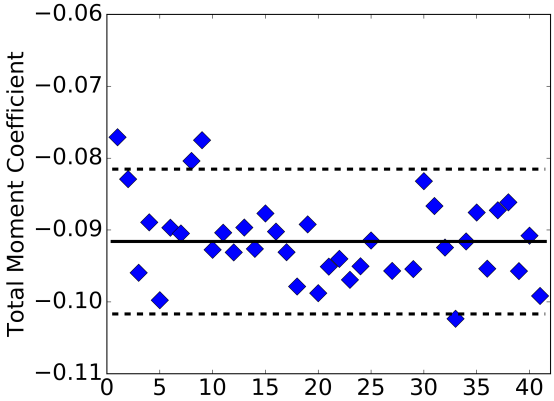

(e) Pitching moment coefficient

Figure 13: Coarse (L2) grid measures of interest for Case 2A.

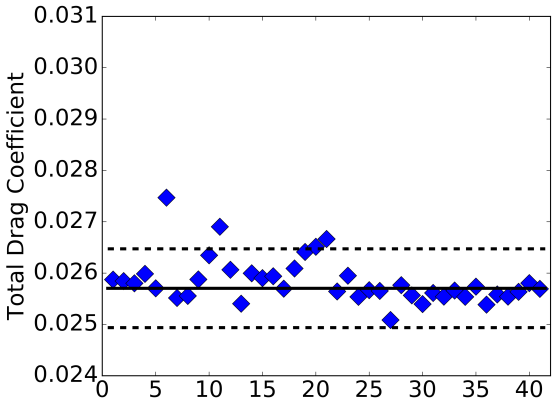

(a) Total drag coefficient

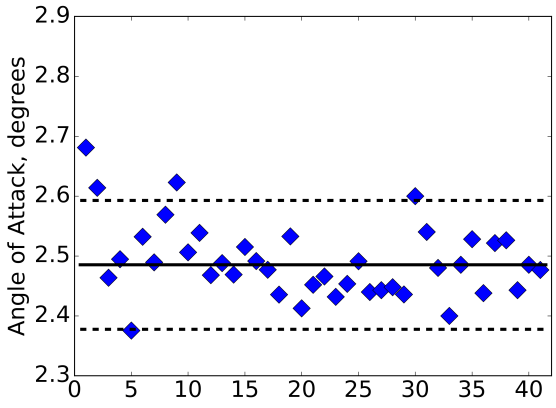

(b) Angle of attack

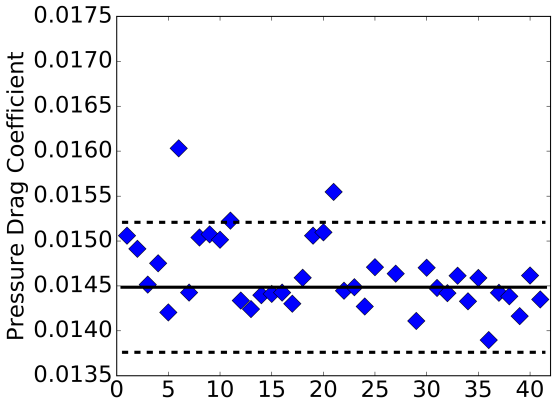

(c) Pressure drag coefficient

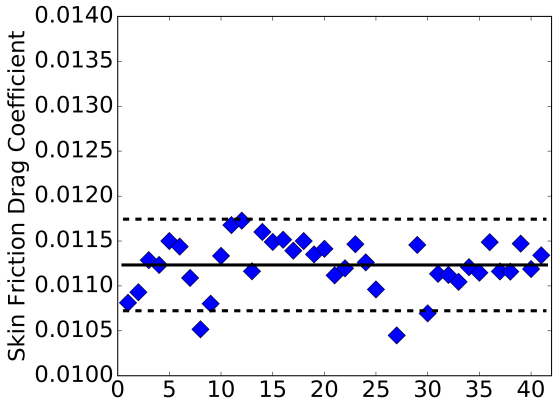

(d) Skin friction drag coefficient

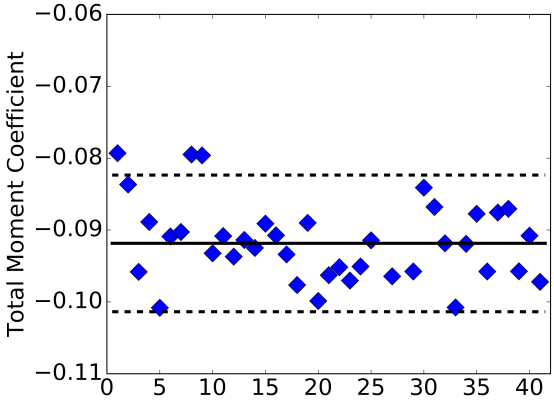

(e) Pitching moment coefficient

Figure 14: Medium (L3) grid measures of interest for Case 2A.

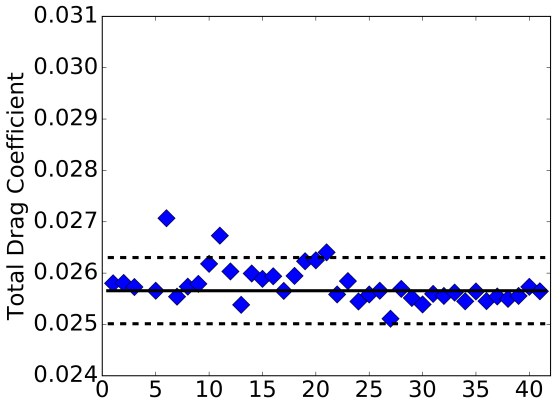

(a) Total drag coefficient

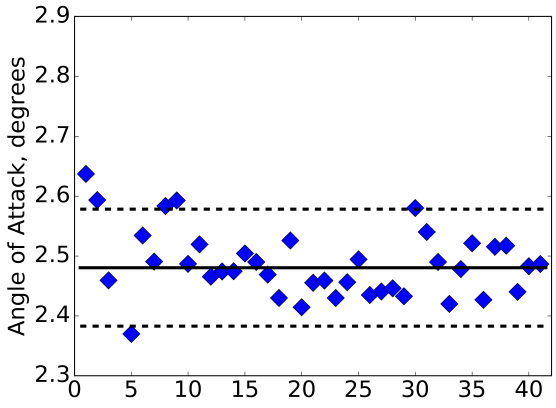

(b) Angle of attack

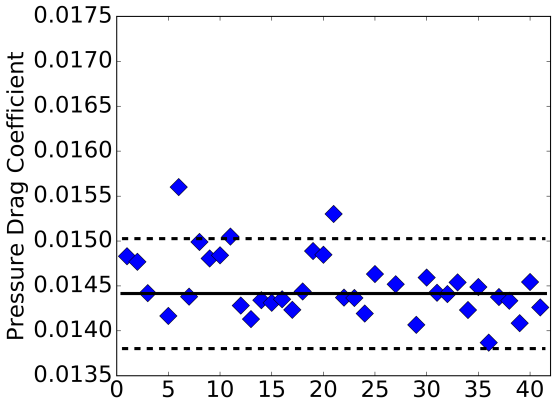

(c) Pressure drag coefficient

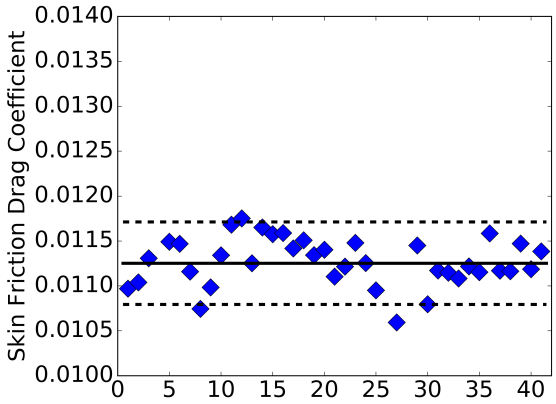

(d) Skin friction drag coefficient

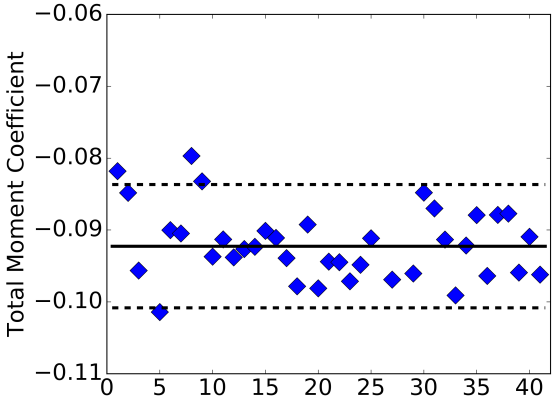

(e) Pitching moment coefficient

Figure 15: Fine (L4) grid measures of interest for Case 2A.

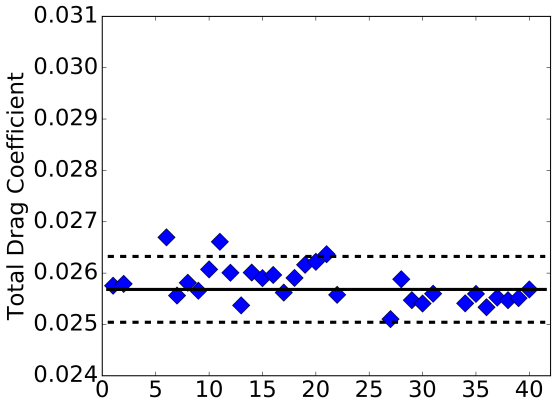

(a) Total drag coefficient

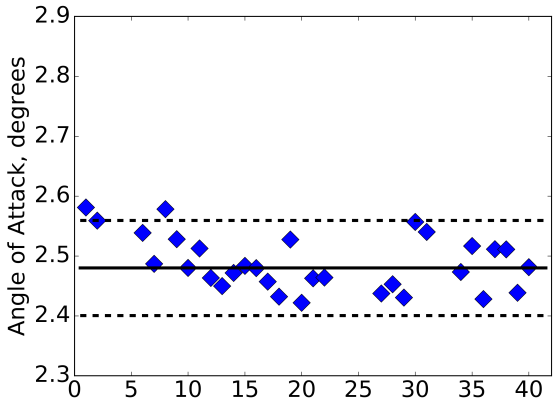

(b) Angle of attack

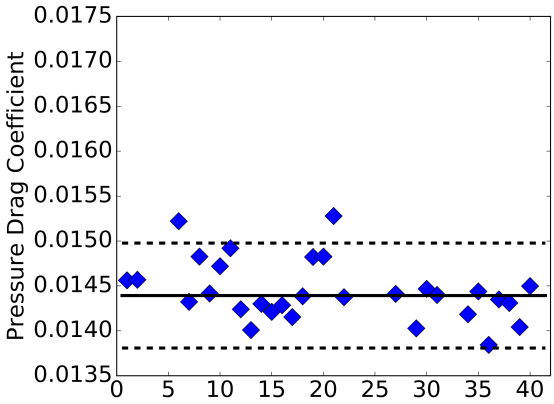

(c) Pressure drag coefficient

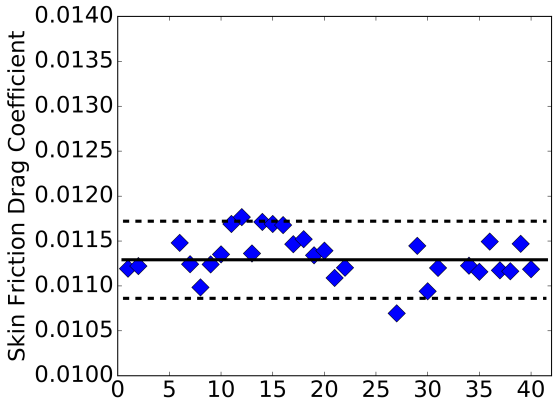

(d) Skin friction drag coefficient

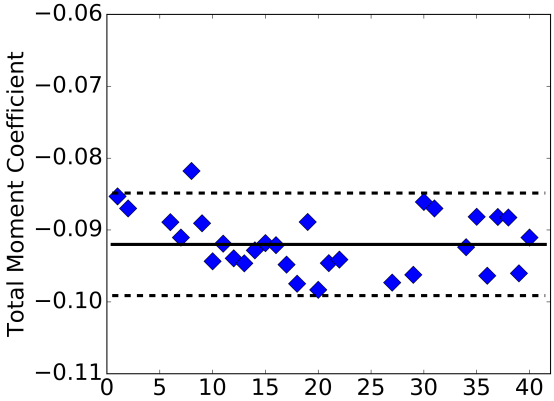

(e) Pitching moment coefficient

Figure 16: Extra Fine (L5) grid measures of interest for Case 2A.

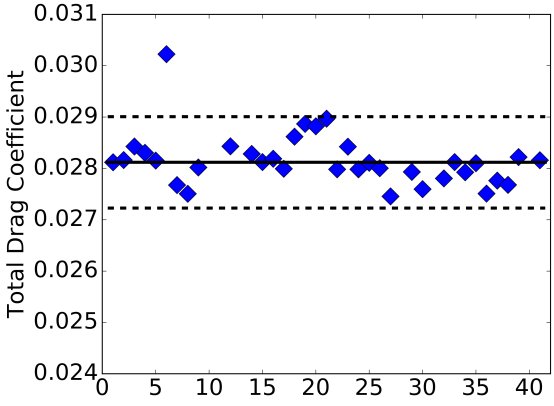

(a) Total drag coefficient

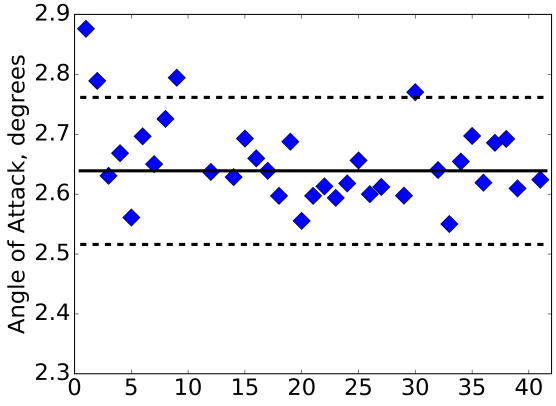

(b) Angle of attack

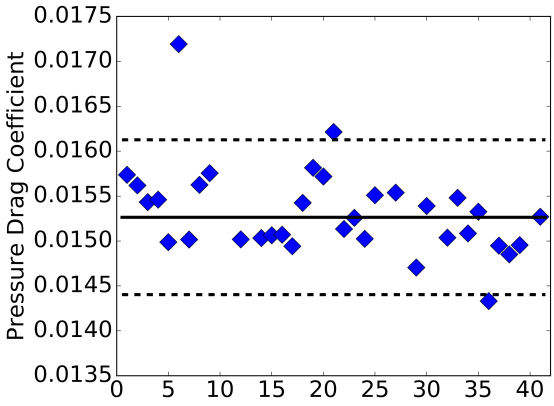

(c) Pressure drag coefficient

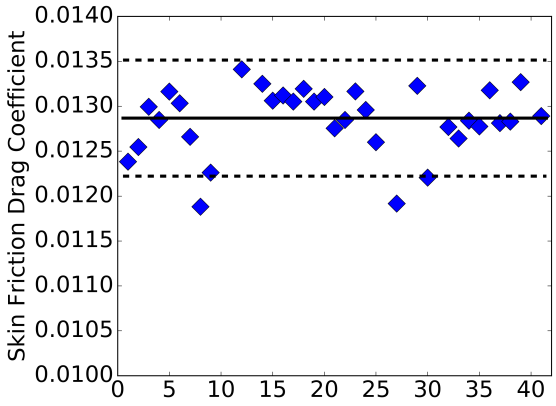

(d) Skin friction drag coefficient

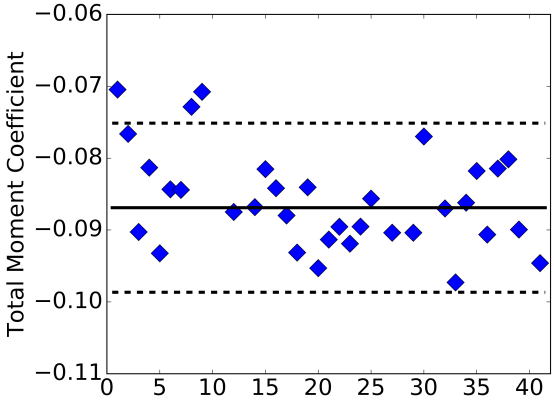

(e) Pitching moment coefficient

Figure 17: Coarse (L2) grid measures of interest for Case 2B.

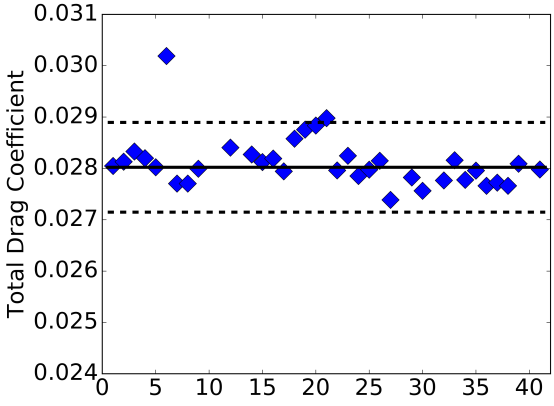

(a) Total drag coefficient

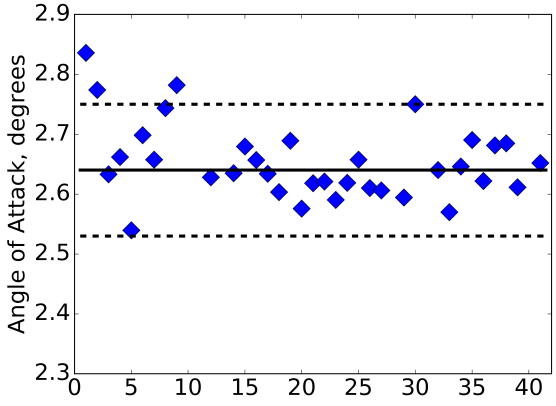

(b) Angle of attack

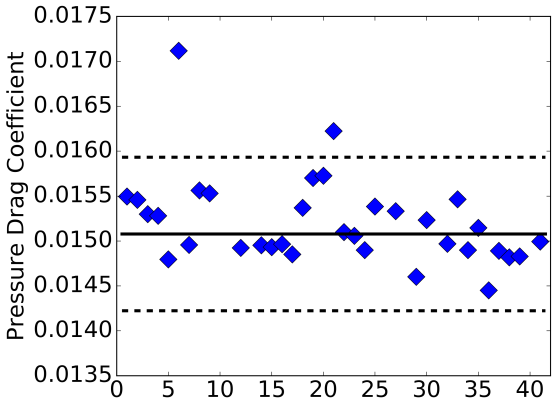

(c) Pressure drag coefficient

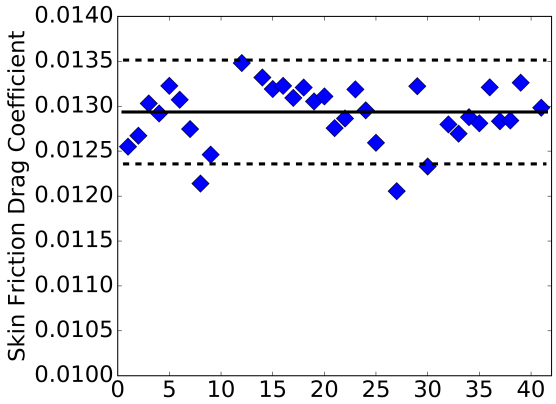

(d) Skin friction drag coefficient

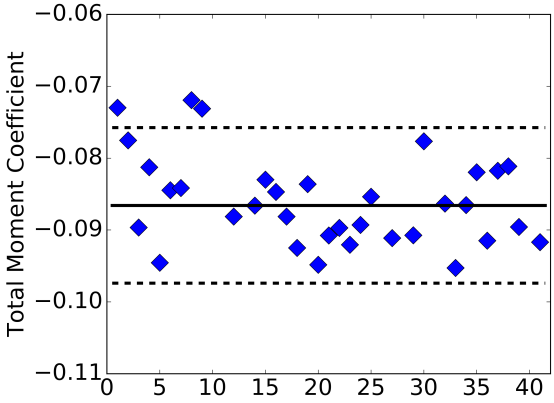

(e) Pitching moment coefficient

Figure 18: Medium (L3) grid measures of interest for Case 2B.

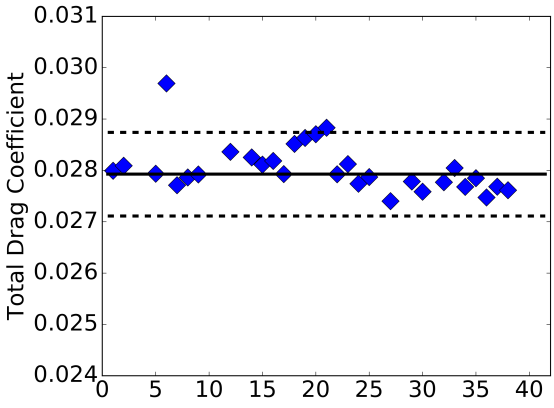

(a) Total drag coefficient

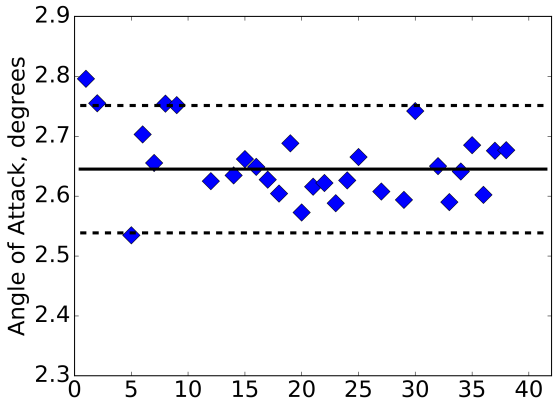

(b) Angle of attack

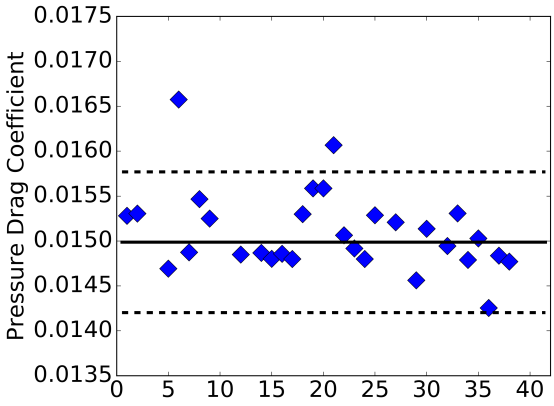

(c) Pressure drag coefficient

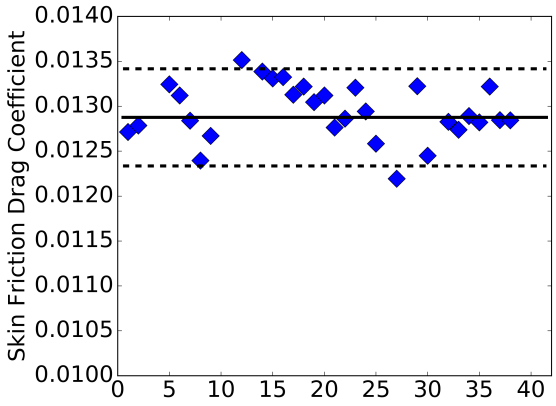

(d) Skin friction drag coefficient

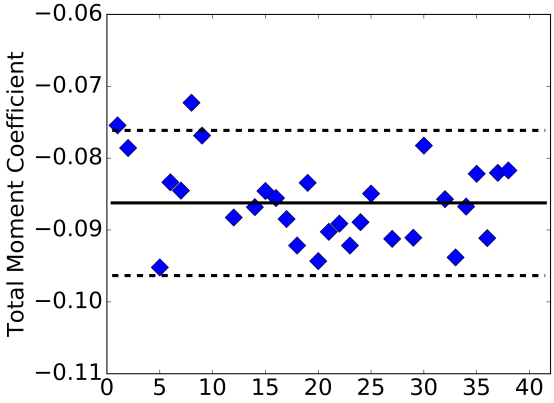

(e) Pitching moment coefficient

Figure 19: Fine (L4) grid measures of interest for Case 2B.

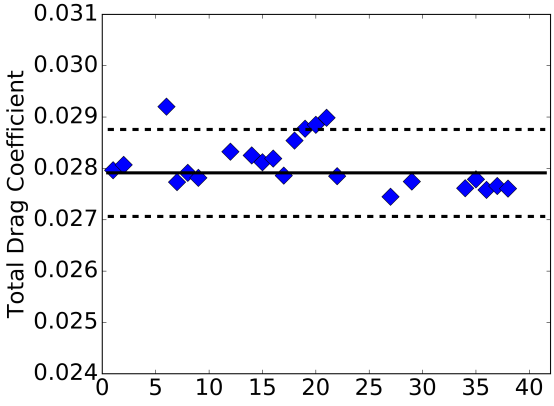

(a) Total drag coefficient

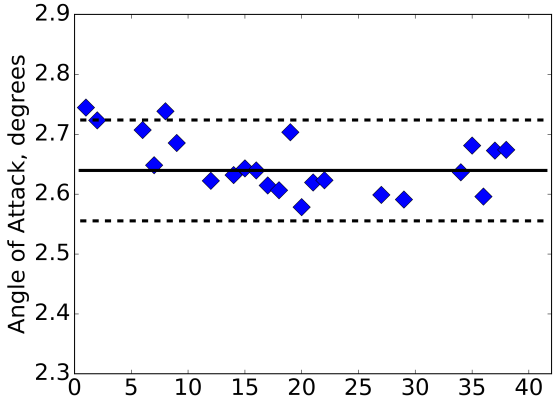

(b) Angle of attack

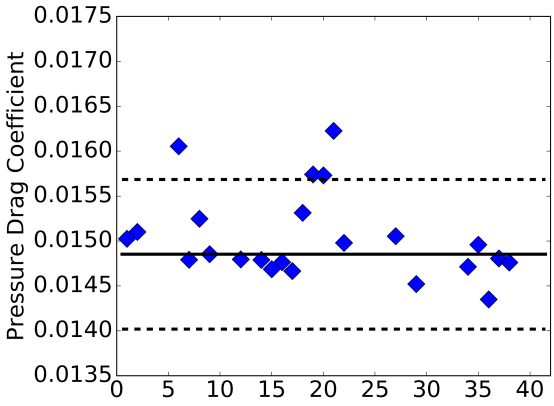

(c) Pressure drag coefficient

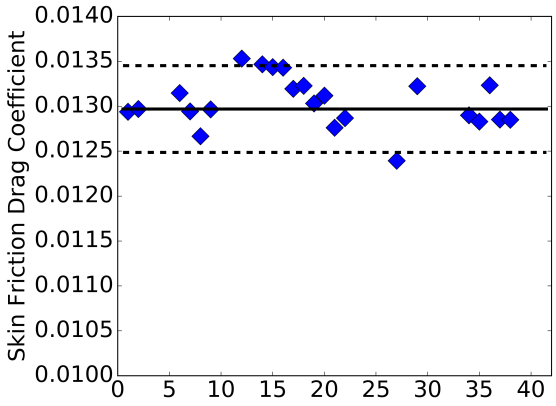

(d) Skin friction drag coefficient

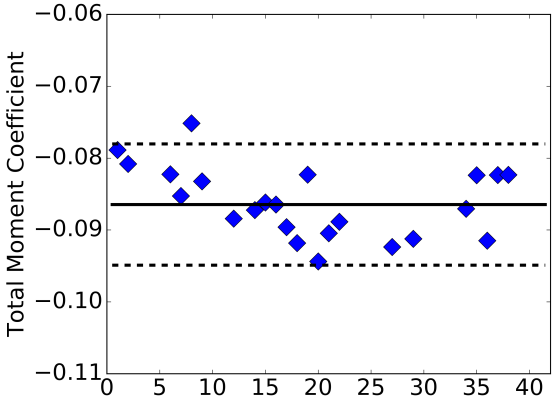

(e) Pitching moment coefficient

Figure 20: Extra Fine (L5) grid measures of interest for Case 2B.

Acknowledgments

The authors wish to thank the participants of the DPW series who have spent countless hours making this series of workshops a continuing success. The authors wish to thank the members of the DPW Organizing Committee for their comments and support. This work was supported by the Revolutionary Vertical Lift Technology (RVLT) Project of the NASA Advanced Air Vehicles Program.

References

[1]Levy, D., Zickuhr, T., Vassberg, J., Agrawal, S., Wahls, R. A., Pirzadeh, S., and Hemsch, M. J., "Data Summary from the First AIAA Computational Fluid Dynamics Drag Prediction Workshop," *Journal of Aircraft*, Vol. 40, No. 5, 2003, pp. 875–882.

[2]Hemsch, M. J., "Statistical Analysis of Computational Fluid Dynamics Solutions from the Drag Prediction Workshop," *Journal of Aircraft*, Vol. 41, No. 1, 2004, pp. 95–103.

[3]Laflin, K. R., Klausmeyer, S. M., Zickuhr, T., Vassberg, J. C., Wahls, R. A., Morrison, J. H., Brodersen, O. P., Rakowitz, M. E., Tinoco, E. N., and Godard, J.-L., "Data Summary from the Second AIAA Computational Fluid Dynamics Drag Prediction Workshop," *Journal of Aircraft*, Vol. 42, No. 5, 2005, pp. 1165–1178.

[4]Hemsch, M. J. and Morrison, J. H., "Statistical Analysis of CFD Solutions from 2nd Drag Prediction Workshop," AIAA Paper 2004-0556, January 2004.

[5]Vassberg, J. C., Tinoco, E. N., Mani, M., Brodersen, O. P., Eisfeld, B., Wahls, R. A., Morrison, J. H., Zickuhr, T., Laflin, K. R., and Mavriplis, D. J., "Summary of the Third AIAA CFD Drag Prediction Workshop," AIAA Paper 2007-0260, January 2007.

[6]Morrison, J. and Hemsch, M., "Statistical Analysis of CFD Solutions from the Third AIAA Drag Prediction Workshop," AIAA Paper 2007-0254, January 2007.

[7]Vassberg, J., Tinoco, E. N., Mani, M., Zickuhr, T., Levy, D. W., Brodersen, O. P., Eisfeld, B., Wahls, R. A., Morrison, J. H., Mavriplis, D. J., and Murayama, M., "Summary of the Fourth AIAA CFD Drag Prediction Workshop," AIAA Paper 2010-4547, June 2010.

[8]Morrison, J., "Statistical Analysis of CFD Solutions from the Fourth AIAA Drag Prediction Workshop," AIAA Paper 2010-4673, June 2010.

[9]Levy, D. W., Laflin, K. R., Tinoco, E. N., Vassberg, J. C., Mani, M., Rider, B., Rumsey, C., Wahls, R. A., Morrison, J. H., Brodersen, O. P., Crippa, S., Mavriplis, D. J., and Murayama, M., "Summary of Data from the Fifth AIAA Computational Fluid Dynamics Drag Prediction Workshop," *Journal of Aircraft*, Vol. 51, No. 4, 2014, pp. 1194–1213.

[10]Morrison, J., "Statistical Analysis of the Fifth Drag Prediction Workshop Computational Fluid Dynamics Solutions," *Journal of Aircraft*, Vol. 51, No. 4, 2014, pp. 1214–1222.

[11]Redeker, G., "DLF-F4 Wing Body Configuration," *A Selection of Experimental Test Cases for the Validation of CFD Codes*, Vol. II, AGARD-AR-303, August 1994, pp. B4.1–B4.21.

[12]Redeker, G., Muller, R., Ashill, P., Elsenaar, A., and Schmitt, V., "Experiments on the DLR-F4 Wing Body Configuration in Several European Wind Tunnels," *Aerodynamic Data Accuracy and Quality: Requirements and Capabilities in Wind Tunnel Testing*, AGARD-CP-429, July 1988.

[13]Elsholz, E., "The DLR-F4 Wing/Body Configuration," *ECARP - European Computational Aerodynamics Research Project: Validation of Turbulence Models, Notes on Numerical Fluid Mechanics*, Vol. 58, 1997, pp. 429–450.

[14]Brodersen, O. P. and Sturmer, A., "Drag Prediction of Engine-Airframe Interference Effects Using Unstructured Navier-Stokes Calculations," AIAA Paper 2001-2414, June 2001.

[15]Vassberg, J., Sclafani, A., and DeHaan, M., "A Wing-Body Fairing Design for the DLR-F6 Model: a DPW-III Case Study," AIAA Paper 2005-4730, June 2005.

[16]Gatlin, G. M., Rivers, M. B., Goodliff, S. L., Rudnik, R., and Sitzmann, M., "Experimental Investigation of the DLR-F6 Transport Configuration in the National Transonic Facility (Invited)," AIAA Paper 2008-6917, August 2008.

[17]Vassberg, J. C., DeHaan, M. A., Rivers, S. M., and Wahls, R. A., "Development of a Common Research Model for Applied CFD Validation Sudies," AIAA Paper 2008-6919, August 2008.

[18]Rivers, M. B. and Dittberner, A., "Experimental Investigations of the NASA Common Research Model (Invited)," AIAA Paper 2010-4218, June 2010.

[19]Rivers, M., Hunter, C., and Campbell, R., "Further Investigation of the Support System Effects and Wing Twist on the NASA Common Research Model," AIAA Paper 2012-3209, June 2012.

[20]Hue, D., "Fifth Drag Prediction Workshop: ONERA Investigations with Experimental Wing Twist and Laminarity," *Journal of Aircraft*, Vol. 51, No. 4, 2014, pp. 1311–1322.

[21]*U.S. Guide to the Expression of Uncertainty in Measurement*, ANSI/NCSL Z540.2-1997, October 1997.

[22]McGill, R., Tukey, J., and Larsen, W., "Variations of Box Plots," *The American Statistician*, Vol. 32, No. 1, 1978, pp. 12–16.

[23]Roy, C., "Summary of Data from the Sixth AIAA CFD Drag Prediction Workshop: Case 1 Code Verification," AIAA Paper to be published, January 2017.

[24]Wheeler, D., *Advanced Topics in Statistical Process Control*, SPC Press, Knoxville, TN, 1995.